forests

MDPI

Article

Automatic Processing for Identification of Forest Fire Risk Areas along High-Voltage Power Lines Using Coarse-to-Fine LiDAR Data

David Hernández-López [1], Jorge López-Rebollo [2], Miguel A. Moreno [1] and Diego Gonzalez-Aguilera [2,*]

[1] Institute for Regional Development, University of Castilla-La Mancha, Campus Universitario s/n, 02071 Albacete, Spain
[2] Department of Cartographic and Land Engineering, Higher Polytechnic School of Ávila, University of Salamanca, Hornos Caleros, 50, 05003 Ávila, Spain
* Correspondence: daguilera@usal.es

Abstract: This work focuses on the automatic identification of forest fire risk areas along high-voltage power lines through the development of a tool and its validation on a real forest area. The tool allows one to automate the whole process, which includes the classification of the point cloud, the computation of the catenary of the wires using different calculation methods, the estimation of the vegetation growth and the identification of the risk areas. To this end, a coarse-to-fine approach is proposed, so that a preliminary analysis is performed with public airborne LiDAR data, and then a more detailed inspection is provided with drone LiDAR data over those areas classified as high risk. The tool and the methodology developed were validated along a high-voltage power line of 53 km in a real forest area. The results show that although the preliminary analysis based on public airborne LiDAR data is more conservative, it is very useful for selecting those areas of higher risk for further analysis with drone LiDAR data.

Keywords: forest fires; electrical fires; risk analysis; power lines; LiDAR; software development

check for updates

Citation: Hernández-López, D.; López-Rebollo, J.; Moreno, M.A.; Gonzalez-Aguilera, D. Automatic Processing for Identification of Forest Fire Risk Areas along High-Voltage Power Lines Using Coarse-to-Fine LiDAR Data. *Forests* **2023**, *14*, 662. https://doi.org/10.3390/f14040662

Academic Editor: Palaiologos Palaiologou

Received: 2 March 2023
Revised: 20 March 2023
Accepted: 21 March 2023
Published: 23 March 2023

Copyright: © 2023 by the authors. Licensee MDPI, Basel, Switzerland. This article is an open access article distributed under the terms and conditions of the Creative Commons Attribution (CC BY) license (https://creativecommons.org/licenses/by/4.0/).

1. Introduction

The high demand for energy requires an electricity transmission grid that is growing year by year. By the end of 2021, there were already more than 44,000 km of high-voltage lines in Spain [1]. These infrastructures involve a modification of the natural environment and often require crossing forest areas that are affected by their construction, making it necessary to have a protection zone to avoid service interruptions and possible forest fires [2]. However, the conservation and monitoring of these protection areas are complicated due to their length, their orography and especially the difficult access in many cases, as traditionally the inspection of power lines has been carried out by means of field surveys [3]. This lack of maintenance poses a risk both of forest fires and for the continuity of service in the event of a possible system failure, as in many cases it is a fire generated by other causes that could affect the power line [4]. Although this type of infrastructure causes fewer forest fires than other ignition sources [5], its detection and response is more complicated, being able to affect larger areas [6,7]. In addition, extreme natural phenomena such as geomagnetic storms can cause huge forest fires that have historically affected power lines [8–11]. Moreover, such fires can be exacerbated by solar activity, such as those that occurred during 2018 in California, Portugal and Greece [12]. For these reasons, high-voltage power lines can represent a hazard by causing or increasing the intensity of forest fires. It is, therefore, important to carry out the correct maintenance of power lines and ensure that these protection areas are cleaned of vegetation, thus avoiding the generation of fuel models in accordance with current regulations [13].

To carry out the maintenance of these areas, different techniques have been applied to automate the process of both detecting power lines and monitoring the state of the

vegetation [14]. Satellite-based remote sensing information can be used for estimating the height of vegetation [15] or classifying burnt areas [16]. If more detail is needed, airborne LiDAR can be also used for characterizing and modelling power lines [17] as well as for monitoring surrounding vegetation [18], especially in those countries where end users can have access to open data based on LiDAR [19]. More recently, simultaneous location and mapping (SLAM) techniques have been used to provide an automatic and detailed inventory of forest areas [20], although the detail of these techniques is excessive for this application. Of course, aerial drones have been used to this end, thanks to advances in platforms and sensors [21]. The most recent studies tend to use LiDAR devices on-board, as they provide a higher density of points and especially good performance for digitization of power lines and calculation of vegetation heights and volumes to estimate fuel models [22]. Other types of data such as synthetic aperture radar [23] or hyperspectral imagery [24] can be obtained from on-board sensors to perform soil moisture calculations and improve simulation models for forest fire prediction. However, the main limitation of these on-board sensors on drones is their reduced autonomy, making the recording of large forest areas difficult.

Regarding forest fire risk assessment models, although some studies have been carried out in an effort to prevent ignition risk by analysing the time-frequency factor of the power line itself [25], most of them use indices or classification systems based on meteorological, topographical, or vegetation parameters [26]. In this sense, regression models that combine these parameters with moisture indices, human factors, or lightning probability [27–29] have been developed and integrated into geographical information systems (GIS) to obtain ignition and spread maps that serve as a predictive tool for firefighting [30].

Although many of these studies incorporate vegetation factors as mentioned above, most of them are theoretical indices without field data for their validation. Some authors deal with LiDAR data acquisition from manned airborne or drone platforms. However, the models are generated and the validation generally carried out in small areas with power lines of less than 1 km in length [3,31,32]. Therefore, to date, there has been a need for the development of a fully automatic methodology for detecting, extracting, and analysing forest risk areas on a large scale.

In this paper, an automatic approach for the assessment of large forest fire risk areas along high-voltage power lines is proposed and validated. The study focuses on the analysis of the geometry of both the power line wiring and the physical environment (i.e., vegetation and ground). To this end, the proposed methodology uses two types of input data based on LiDAR: (i) public LiDAR data coming from an airborne mission [13]; and (ii) self-generated LiDAR data coming from a drone flight. In particular, a coarse-to-fine approach has been implemented for the detection, extraction, and analysis of these forest fire risk areas. In the first level, public airborne LiDAR data are used to automate the detection and extraction of these areas with some theoretical considerations about the power lines according to the regulations. In a second level, a more detailed analysis of those areas of higher risk is carried out, using drone LiDAR data and more accurate modelling of the power lines. In addition, a predictive model is proposed to estimate the growth of vegetation through time and thus to estimate the forest fire risk areas in the near future. This twofold approach is very cost-efficient in those countries that integrate in their cartographic plans the periodic acquisition of LiDAR flights, as is the case in Spain with the PNOA-LiDAR project [19].

This paper presents the following structure: after this introduction, Section 2 describes the types of data used and the methodology developed to carry out the calculation and assessment of the forest fire risk areas. Section 3 shows the experimental results obtained from the application of the tool developed over a real forest area and discusses the different results obtained. Finally, Section 4 presents the conclusions as well as future works.

2. Materials and Methods

The methodology developed for the calculation of forest fire risk areas along high-voltage power lines takes public LiDAR data [19] and drone LiDAR data as input. The

main goal of the methodology is to use available public LiDAR data to analyse entire power lines in an automated way and to extract areas of risk where it could be appropriate to use drone LiDAR data to carry out a detailed analysis. The methodology also can be applied in those cases where only one type of data is available.

This proposed methodology consists of a set of plugins developed within QGIS and supported by the LAStools library [33]. The automatic workflow for obtaining the forest fire risk areas was divided into two main modules (Figure 1): (i) the processing of the point cloud to obtain an optimised point cloud, eliminating data that are out of the region of interest (ROI) and reducing the density on some types of surface (e.g., ground); (ii) the computation and mapping of the forest fire risk areas based on extraction of the wire catenary, the estimation of their position under different load hypotheses, and the application of a vegetation growth model.

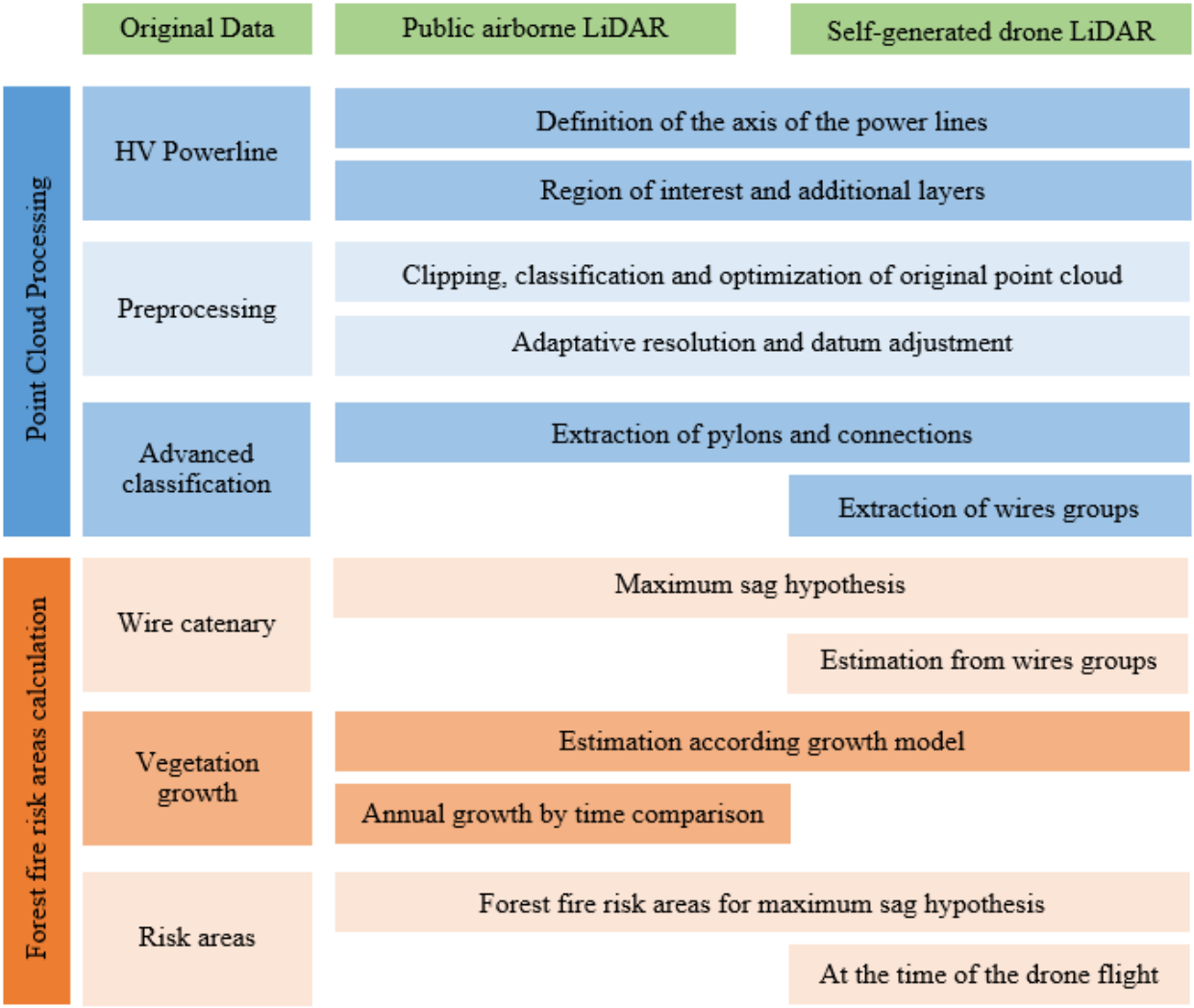


Figure 1. Automatic workflow for the identification of forest fire risk areas along high-voltage power lines using LiDAR data processing.

Figure 1 shows the process workflow, outlining the steps to be followed for each module. It should be noted that processes applied to both datasets (public LiDAR data, self-generated drone LiDAR data) are similar, with the particularity that the drone LiDAR data provides higher spatial resolution, so it is possible to apply some advanced processing to refine the results obtained. In addition, more precise and reliable results can be obtained regarding the state of the power line and the vegetation at the time of the drone flight.

2.1. Input Data

2.1.1. Public Airborne LiDAR Data

The National Aerial Orthophotography Plan (PNOA) is an initiative that aims to obtain free and public digital cartography of the entire country. In particular, the PNOA-LiDAR project started in 2009 to obtain point clouds captured with an airborne LiDAR sensor (Table 1). Two coverages of the Spanish territory have been carried out: the first one between 2009–2015 and the second one from 2015 [34].

Table 1. Technical specifications of the public airborne LiDAR data.

Specifications	First Coverage	Second Coverage
Minimum point density	0.5 points/m^2	0.5–2 points/m^2
Flying years	2009–2015	2015–
Geodetic reference system	ETRS89 28th, 29th, 30th and 31st zones	
Height reference system	Orthometric altitudes, reference geoid: EGM08	
RMSE Z	≤40 cm	≤20 cm
Estimated planimetric accuracy	≤30 cm	≤30 cm

The methodology developed uses these input data, which are freely accessible from the website of the National Centre for Geographic Information (CNIG) [35], being available in LAZ or LAS format [36] with an extension of 2 × 2 km.

2.1.2. Public Power Line Data

Each country has institutions or companies responsible for the maintenance of electricity infrastructures that manage the high-voltage electricity transmission network in accordance with legislation, as is the case with "Red Eléctrica Española" in Spain. The information on these infrastructures is generally available to the public, as is the case with the National Geographic Institute (IGN), which is responsible for mapping the electricity grid through the National Topographic Base (BTN), and can be downloaded in vector format through the CNIG [35]. It is possible to access information related to the voltage or typology of the power lines for the entire national territory.

On the other hand, public initiatives such as the Hierarchical INSPIRE Land Use Classification System (HILUCS) in Europe provide land use mapping. One of these public databases is the High-Resolution Spanish Land Use Information System (SIOSE AR) [37]. The information on land use allows the delimitation of the electricity network, restricting the power lines only to forest areas, which are the subject of this study.

2.1.3. Self-Generated Drone LiDAR Data

Optionally, the tool can use other sources of LiDAR data with better spatial resolution. Phoenix LiDAR Systems' Scout Ultra equipment (Phoenix LiDAR Systems, Austin, TX, USA) (Figure 2) was used for data capture in the case study presented in this paper. Drone LiDAR data (Table 2) provide point clouds with a density of more than 300 points/m^2 and a range of 200 m, being the perfect complement to analyse in detail those areas with higher risk.

Table 2. Technical specifications of the self-generated drone LiDAR data.

Specifications	Value
Laser properties	905 nm Class 1 (eye safe)
Number of lasers	32
Range min/max/resolution	1.0 m/200 m/4 mm
Max effective measurement ratio	600,000 meas./s
Horizontal/Vertical FoV	360°/40° (−25° to +15°)
Absolute accuracy	55 mm RMSE @ 50 m range



Figure 2. Scout Ultra LiDAR sensor on-board Phoenix drone platform.

2.2. Automatic Analysis of Forest Fire Risk Areas along High-Voltage Power Lines

2.2.1. High-Voltage Power Lines Definition

Although the power lines are imported as input data and stored in a geospatial database in shapefile format, there is no three-dimensional information about the electricity network (e.g., the height of pylons). Nevertheless, this bidimensional input is used to define the components and their location and subsequently carry out the segmentation and classification of the point cloud.

As a result, the high-voltage power line, expressed as a 2D polyline, is used in such a way that its vertices correspond to the position of each pylon, whereas the lines between vertices define the axis of the power line.

Once the high-voltage power line has been imported and labelled, a region of interest (ROI) is automatically generated using a buffer of 120 m, taking the axis of the power line as a reference. This allows segmenting the point cloud for working only with the surrounding power line environment. Furthermore, within this ROI, three more buffers are generated using the axis of the power line as reference: (i) a buffer of 25 m for the processing of public airborne LiDAR data; (ii) a buffer of 15 m for the processing of self-generated drone LiDAR data, due to its higher resolution; (iii) a buffer of 7.5 m for isolating the wires and the pylons during the classification of the vegetation that is explained in Section 2.2.3.

2.2.2. Preprocessing

Once the power line is defined, the next step is to preprocess the point clouds. To do this, the raw data can be downloaded automatically thanks to the ROI defined above, which is used to access the CNIG database and obtain the corresponding LAZ files.

The point clouds are preprocessed using an adaptative resolution and a coordinate reference system (CRS). In particular, a datum adjustment is applied to work with the same height reference system (i.e., orthometric altitudes). Additionally, a specific function is developed for providing an adaptative resolution along the power lines (e.g., higher resolution in the ROI of 7.5 m).

Next, a filtering of the point cloud is carried out, removing noise that could affect the point cloud classification. For this purpose, a neighbouring point isolation approach is applied [38] (e.g., if in a 10 × 10 × 10 m cube a point has less than 6 neighbours, it is considered as noise, and it is eliminated).

Once the point cloud has been filtered, it is preclassified into two single classes: ground and unclassified points. This preclassification is performed for the whole ROI corresponding to the 120 m buffer.

The result of this preprocessing consists of a single LiDAR point cloud preclassified into two classes, which are used as input in the rest of the processes. Together with this preclassified point cloud, a digital terrain model (DTM) in raster format is derived from the ground class, which is used as the reference to calculate the heights on the ground in the rest of the proposed methodology.

2.2.3. Advanced Point Cloud Classification

The next step consists of classifying the point clouds with a twofold goal: isolate the elements of interest, avoiding false positives; and provide a fine classification of pylons and wires.

The advanced point cloud classification is carried out using a random forest [39] algorithm focused on the extraction of pylons and wire groups. In particular, it is trained and classified with the CGAL random forest algorithm [40], using only geometrical features based on the ETH Zurich version of the random forest algorithm [41]. It uses parameters related to their geometrical dimensions obtained from its eigenvalues to generate the training data: sum of eigenvalues, omnivariance, eigenentropy, linearity, planarity, sphericity, anisotropy, and change of curvature. In this way, each of the classes (pylons and wires) has a unique signature in the feature space. Thus, class labels are assigned for each analysed segment according to its features. Initially, those points within a cylinder of radius 8 m and height 45 m and centred on the vertices of the power line imported are assigned to the class "pylon". For the wires, a parallelepiped along the axis of the power line is generated with the following dimensions: a width of 16 m (i.e., pylon diameter); a height between 6 m (i.e., minimum wire height according to the Spanish norm) and 45 m (i.e., maximum pylon height). The length of the parallelepiped is adaptively adjusted from the length between the vertices of the power line imported.

It should be noted that this advanced classification of point cloud provides different results depending on the input data: for public airborne LiDAR data, this process only classifies the points corresponding to the pylons, since there are few points that belong to wires. On the contrary, for self-generated drone LiDAR data, the advanced point cloud classification goes one step further, allowing the extraction of wire groups thanks to the fine resolution of this data source.

For this purpose, the points of each connection are obtained and classified using a spatial clustering criterion by applying the Euclidean cluster extraction algorithm [42]. In this sense, geometric constraints related to the maximum separation of a point from its cluster and a minimum number of points for each cluster are applied.

2.2.4. Wire Catenary Calculation

The computation of the wire catenary requires calculating the geometry of the wires following a twofold approach (Figure 3): (i) for public airborne data, the theoretical maximum sag hypothesis is computed; (ii) for self-generated drone LiDAR data, the real catenary geometry (at the time of drone flight) is computed based on the points classified in the previous step. As mentioned above, public airborne LiDAR data allow one to obtain a smaller number of points, so only the theoretical maximum sag hypothesis can be estimated. In the case of self-generated drone LiDAR data, the processing can be carried out by extracting the geometry of the wires to estimate the real catenary and refine the calculation of the maximum sag hypothesis thanks to the higher density of points available.

In both cases, this wire catenary estimation is used later to determine the risk areas based on the distances to the points in the cloud that do not belong to any object, and which include the following classes: ground points, low, medium and high vegetation.

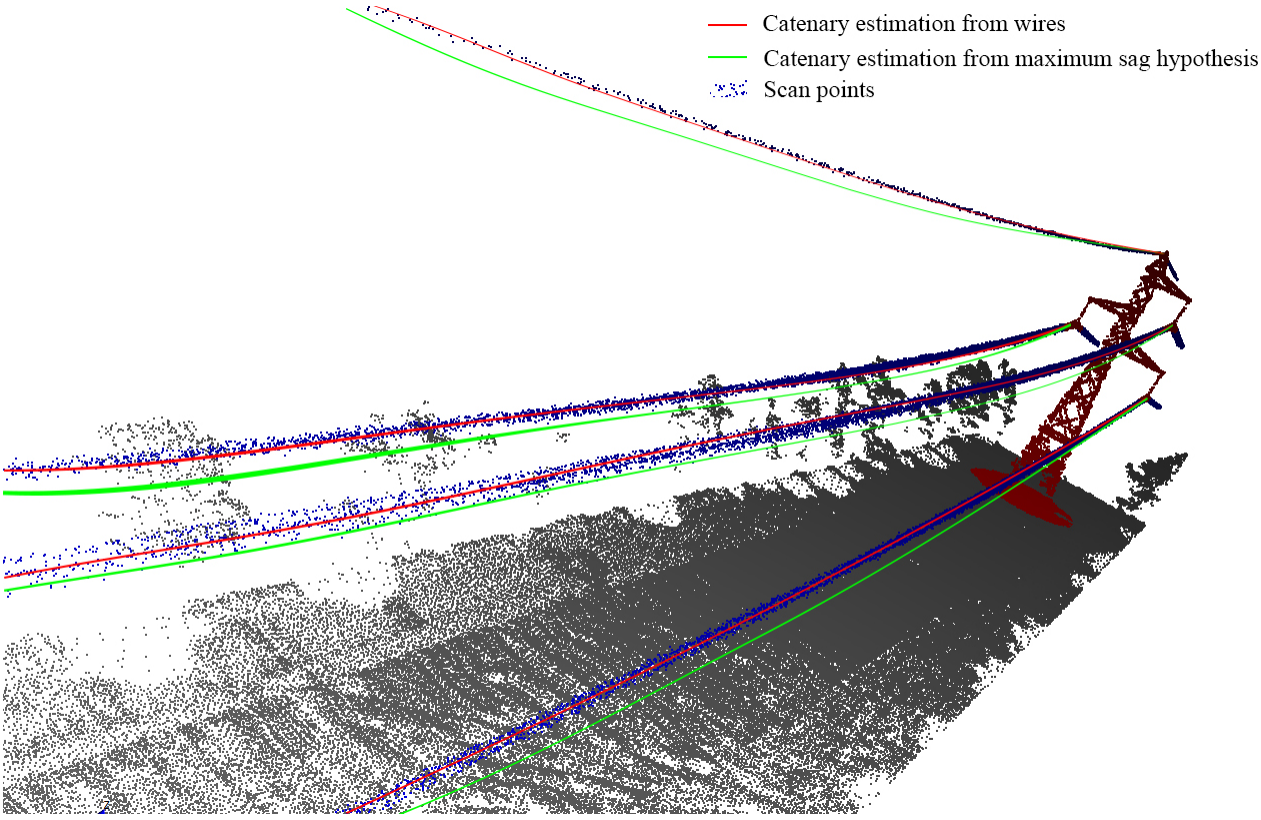


Figure 3. Wire catenary estimation from wire geometry (red) and theoretical maximum sag hypothesis (green). Points classified as cable groups in blue and points classified as pylons in red.

2.2.4.1. Catenary Estimation of Wire Groups Using the Point Cloud

The real catenary estimation from point cloud data can only be calculated using self-generated drone LiDAR data, since the classification in wire groups described in Section 2.2.3 is necessary. In this way, all points included in the "wire" class are used to estimate its 3D geometry (Figure 3). This estimation corresponds to the real catenary geometry for each wire group at the time of drone flight, that is, with the corresponding load and tension conditions and different from the theoretical catenary calculated based on the maximum sag hypothesis. For the real catenary estimation, the algorithm combines least squares adjustment with RANSAC to fit a curve to the classified point cloud of each wire group.

The first step is to determine the 2D line corresponding to the longitudinal profile of each wire group. For this purpose, an iterative least squares process is used to discard outliers. Next, the line is divided into segments by clustering the points every 50 cm to obtain the heights of this longitudinal profile. The average altitude of each segment is obtained by applying RANSAC together with the detection of outliers. In this way, different segments corresponding to each wire group with mean altitude, standard deviation, and number of points are obtained.

For the calculation of the real catenary, the algorithm starts by looking for the anchor points of the wires to the insulators. To do this, five segments obtained from the previous clustering are taken from each of the sides, obtaining the possible catenaries for each of the combinations of these segments, with a total of 25 possible combinations of catenaries.

Then, for each estimated catenary, the deviation is obtained as the difference between its real height (i.e., from the point cloud) and the estimated height with the catenary. The mean value of the error, the standard deviation and the maximum error are calculated for each catenary.

2.2.4.2. Maximum Sag Hypothesis

The theoretical estimation of the catenary based on the maximum sag hypothesis can be used for both types of data (public airborne LiDAR data and self-generated drone LiDAR data). This theoretical approach uses the connection between the pylons as input data. Using this approach, the four groups of wires are simulated for each connection (Figure 4): two lower groups of wires, on each side of the power line axis according to the dimensions of the crossarms and based on the assumption of the minimum height of the wires (6 m), and two upper groups of wires based on the assumption of the maximum height of wires (45 m).

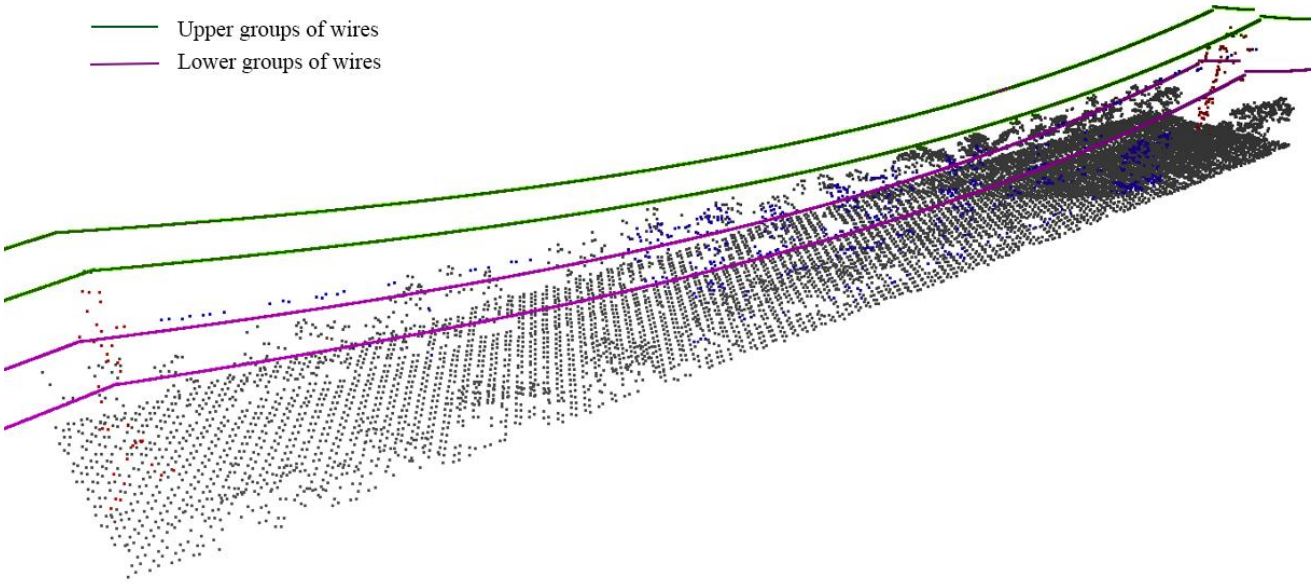


Figure 4. Simulated groups of wires obtained for the theoretical estimation of the catenary based on the maximum sag hypothesis calculation.

The catenary geometry corresponding to the maximum sag hypothesis represents the most unfavourable catenary status, i.e., the catenary condition in which, due to the load and tension conditions, the catenary geometry is more unfavourable. This hypothesis represents the highest risk of forest fire because the wires have a smaller distance to the ground and vegetation. This is why this calculation is of great interest, as it is on the safety side by representing the most extreme event.

Nevertheless, this step requires, as input parameters, the metadata coming from the type of electricity network. In particular, it is necessary to enter the width of the crossarms and the minimum and maximum heights of wires according to the design and safety standards. Last but not least, the type of electricity network, its voltage and the technical specifications of the wire are also required for the theoretical estimation of the catenary based on the maximum sag hypothesis.

These design parameters are used to make a theoretical estimation of the catenary according to its technical specifications together with the 3D position of the two anchor points of the wire to the insulators following an approach similar to the one proposed by Hatibovic [43,44] (Figure 5). The theoretical estimation of catenary was performed using the generic catenary formulation [45] for the case of inclined spans. Although the approach is similar for the two types of data (i.e., public airborne LiDAR and self-generated drone LiDAR), the coordinates of the anchor points are obtained in a different way.

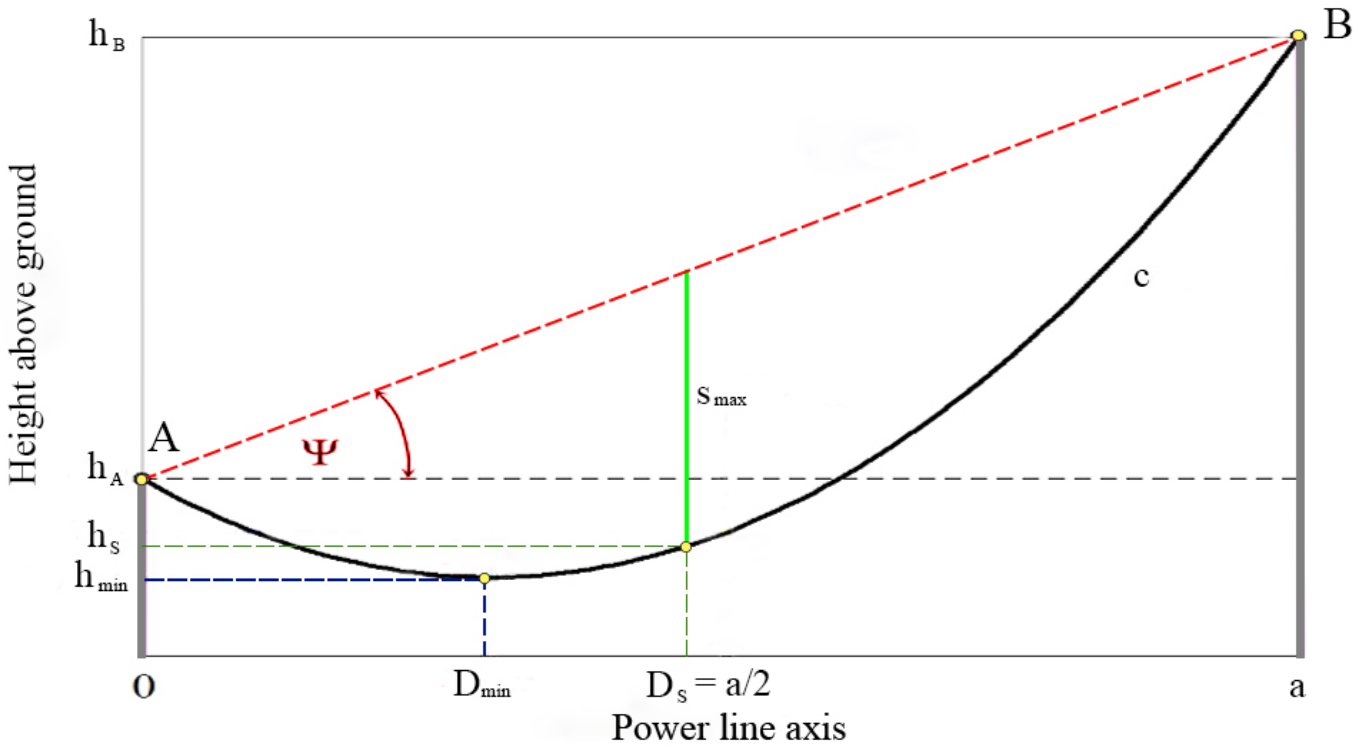


Figure 5. Catenary estimation based on the maximum sag hypothesis with the anchor points at different levels. A and B correspond to the anchor points of the wire to the insulators; Ψ is the angle of inclination between the two points; c is the wire catenary; s_{max} corresponds to the maximum sag; h_{min} is the minimum height of the wires above the ground according to the design standards.

In the case of self-generated drone LiDAR data, the theoretical catenary is calculated for each of the wire groups estimated from the point cloud described in the previous section. In this way, the coordinates of the anchor points are known, as they can be extracted from the previously calculated catenaries.

In the case of public airborne LiDAR data, there is no estimation from the point cloud of these anchor points. To this end, the anchor points are considered at their lowest height (i.e., using the DTM and the height of the ground). To obtain the final height of the catenary, an analysis of the DTM cross sections in the power line axis is automatically performed, and finally, the height corresponding to each of the crossarms in the pylons is determined. The calculated catenaries are then lifted parallel to the ground until their lowest point is at the minimum height above ground determined by the standard according to the type of cable [13].

2.2.5. Vegetation Growth Model

To extrapolate the presence of forest risk areas in the future, it is necessary to use a vegetation growth model along the power line environment. This model can be applied thanks to the approach developed, being necessary to have the LiDAR data classified, at least, in the following classes: ground, medium and high vegetation. In addition, it is necessary to define the electricity network described in Section 2.2.1, as well as the main ROI with the buffer of 120 m. The tool developed allows automating this process within the main ROI as follows.

Firstly, the height of the vegetation is obtained, taking the DTM as reference. Secondly, the main ROI is divided into a grid with cells of 10 × 10 m, for which a statistical analysis of the vegetation heights is performed, eliminating those extreme values (i.e., below the 5% percentile and above the 95% percentile). With the remaining values, the mean and the standard deviation of the heights within the cell are estimated. From these values, it is possible to make an estimation according to Richard's vegetation growth model

(Equation (1)), estimating the current age that corresponds to the height obtained from the statistical analysis.

$$h = a \cdot \left(1 - e^{-b \cdot t}\right)^{c} \quad (1)$$

where h is the height of the tree and t is the age of the tree; a, b and c are model parameters associated with each vegetation type. a represents the maximum height of the tree, b is related to the growth rate and c represents the inflection point in the growth curve. In this case, parameters a, b and c can be automatically assigned according to the location from the vegetation typology established in the Forestry Map of Spain [46].

Once the vegetation growth model has been defined, the vegetation height prediction for a future age can be estimated according to Equation (1).

As a result, this vegetation growth model allows estimating the annual growth of the vegetation in case there are no available data captures with sufficient temporal variation (e.g., public airborne LiDAR data is available in Spain with a time lag of 10 years). In those cases with a better temporal resolution of LiDAR data, a more accurate empirical model could be obtained. In addition, a detailed study of the vegetation varieties in the area would allow the selection of parameters a, b and c to obtain a more accurate model. Nevertheless, the main utility of this vegetation growth model is focused on a first operational phase to detect areas of possible fire risk derived from public airborne LiDAR data.

2.2.6. Risk Areas Calculation

Since the final objective of the methodology is the assessment of forest fire risk areas along high-voltage power lines, the last process consists of the estimation of these risk areas. To perform this calculation, three geometric risks (Figure 6) are used [13]:

1. **Height risk**: focused on the vegetation under the power line (Figure 6a). This first criterion is conditioned by the existence of vegetation under the power line and in adjacent areas, based on the assumption of a possible lateral displacement of the wires by the wind. Areas with higher vegetation may cause interruptions in the system or risk of fire due to the presence of branches close to the wires. In this case, the vegetation growth model is of great interest for extrapolating future calculations, as the height of the vegetation will be estimated according to its growth.
2. **Distance risk**: focused on the vegetation on the sides (Figure 6b). This second criterion analyses the distance to the vegetation on both sides of the power line by calculating the three-dimensional distances from the power line to the closest point of vegetation.
3. **Fall risk**: focused on the possible fall of the vegetation (Figure 6c). This third criterion tries to analyse the risk caused by the fall of vegetation and its possible effect on the power line. In this case, the geometry of the vegetation in 3D would make it possible to determine whether there is possible contact with the power line or whether it would fall at a distance less than the safety distance.

To optimise the processing of the calculation of the risk areas, the algorithm divides the point cloud corresponding to the ROI into a grid of cells of 2 × 2 m for public airborne LiDAR data and cells of 0.5 × 0.5 m for self-generated drone LiDAR data. For each of these cells, the points with the highest height and shortest distance to the power line are calculated, determining whether or not a risk exists according to the three geometric criteria defined above. In addition, the possible outward bending of the wires due to the wind is considered according to the corresponding sag at each point of the catenary.

In the case of self-generated drone LiDAR data, the risk areas are computed from the real catenaries estimated from the point cloud and also from the theoretical catenaries estimated based on the maximum sag hypothesis. In the case of public airborne LiDAR data, the risk areas are computed only with the theoretical catenary based on the maximum sag hypothesis.

Finally, the cells in which at least one of the three risk criteria is detected are stored and grouped in a vector layer that facilitates their geographical representation. For each type of risk, statistics related to the minimum, maximum, mean, standard deviation, and

the number of points are obtained. The results of the risk areas are stored in a spatial database with a simple data model that allows both their representation and their use for decision-making in prevention actions focused on reducing the risk in these areas.

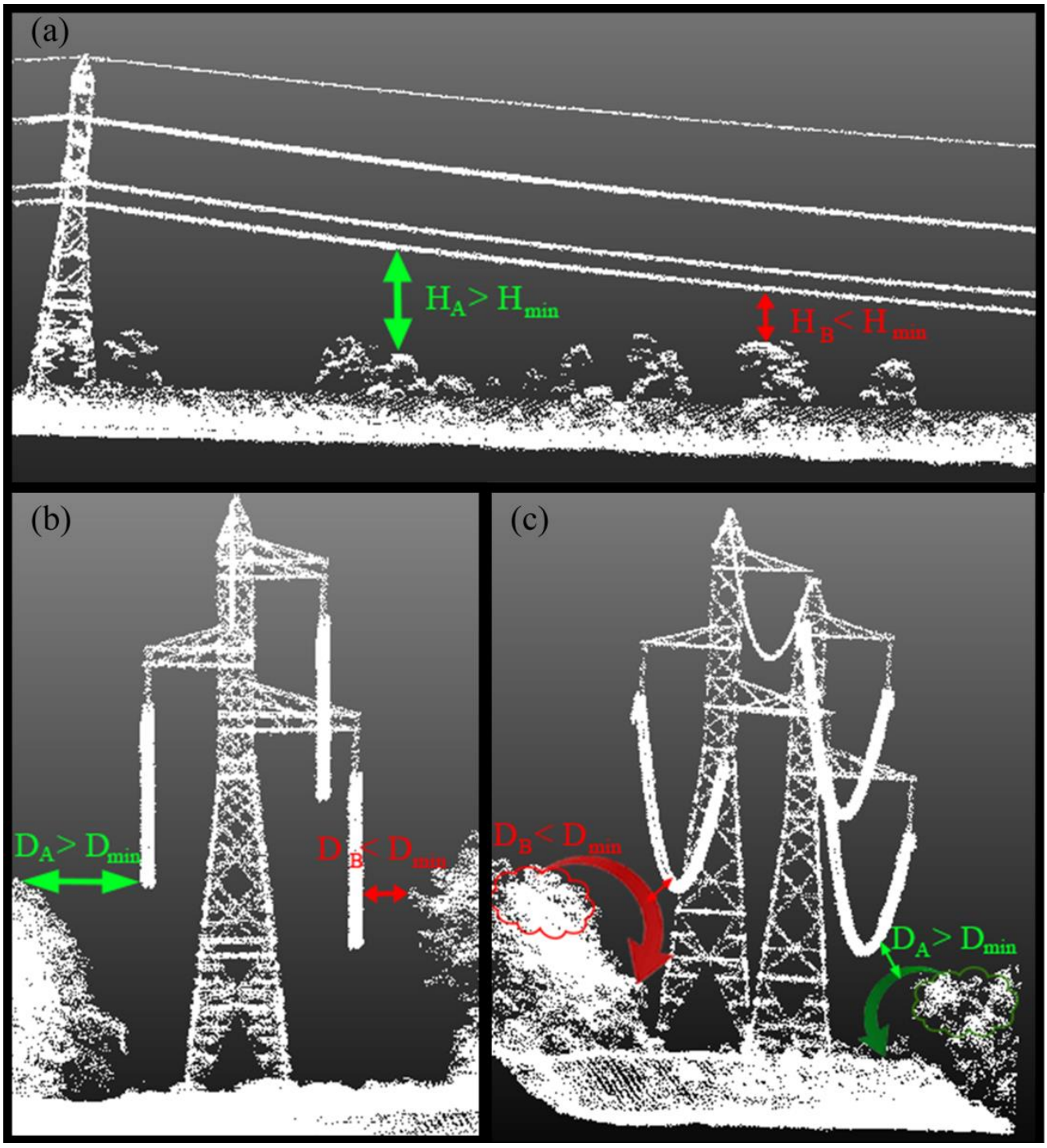


Figure 6. Geometric criteria for defining risk areas: (**a**) Height risk; (**b**) Distance risk; and (**c**) Fall risk. H_{min} and D_{min} correspond to the minimum heights and distances to the vegetation according to the regulations in each country. D_A (green) represents a valid distance, while D_B (red) represents a non-valid distance and thus a risk area.

3. Results and Discussion

3.1. Study Area

To validate the methodology and tool developed, a study area was selected to carry out the processes described above and to obtain the risk areas in this zone.

The study area (Figure 7) corresponds to a 400 kV high-voltage power line with a length of 113 km from the southwest to the northeast of the province of Zamora (Spain). In particular, the section analysed covers a length of 53 km.

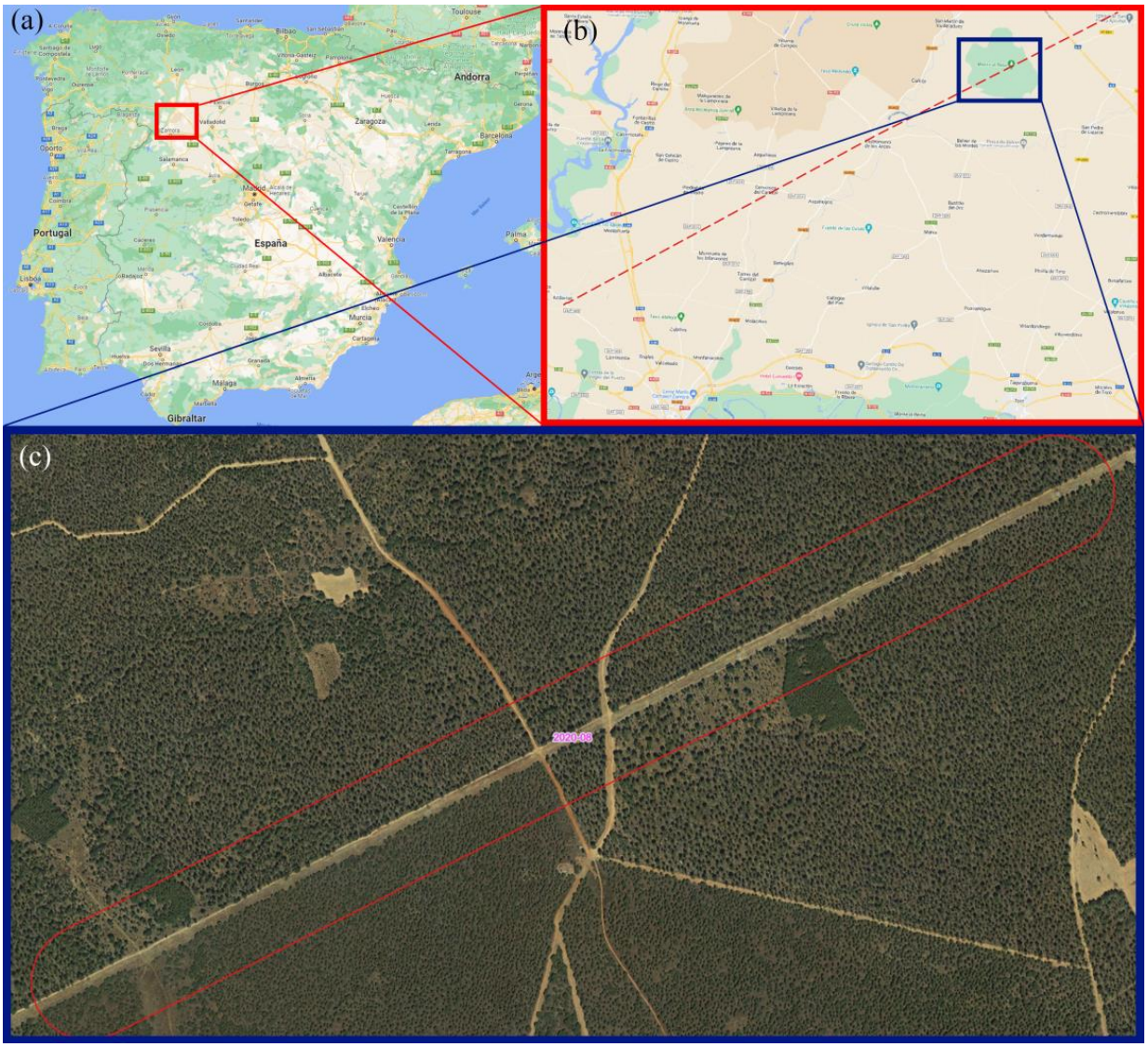


Figure 7. Study area to validate the proposed methodology. (**a**) Location map in Spain; (**b**) situation of the power line in the province of Zamora (Spain); (**c**) selected area for the drone flight.

Due to the higher cost of drone flights, a first approach was carried out using public airborne LiDAR data, so that the processing was performed for the 53 km of power line to determine those risk areas where a more detailed inspection was needed. For this, all of the information was downloaded according to the ROI defined by the power line, including the PNOA LiDAR files in LAZ format corresponding to the year 2019.

Once the risk areas were identified based on public airborne LiDAR data, a drone flight was carried out with the equipment defined in Section 2.1.2. covering this area (Figure 7c) and focusing especially on the area around the power line, which had a length of 2200 m and seven pylons. Self-generated drone LiDAR data were captured in the month of May. The weather was mild, and the vegetation was at its fastest growing time of the year. However, to determine the risk areas, the position of the wires under maximum sag conditions was considered also in this case.

The point clouds were preprocessed with the developed tool according to the steps described in Section 2.2. First, a generic preprocessing was carried out to separate the

ground points from the rest. Then, an advanced classification allowed us to identify the elements of the power line (i.e., pylons and wires). For the public airborne LiDAR data, the points corresponding to the pylons were obtained, while for the drone LiDAR data, the connections between pylons (i.e., anchor points) were also obtained, as the higher density of points made it possible to differentiate the groups of wires.

Once the point cloud was classified and the power line was defined with all of its technical specifications, the wire catenary calculation was carried out using the theoretical maximum sag hypothesis for the public airborne LiDAR data and the twofold approach for the self-generated drone LiDAR data: (i) real catenary estimation of wire groups using the point cloud; (ii) theoretical estimation of the catenary based on the maximum sag hypothesis.

3.2. Results for Public Airborne LiDAR Data

In this case, only the theoretical maximum sag hypothesis was employed to obtain the geometry of the catenary. Following the approach defined in Section 2.2.4.2, the four catenaries for each connection were obtained, as can be seen in Figure 4. In this case, the upper estimated catenaries may present a greater deviation with respect to the real catenary, since in some cases they are not always parallel at the same height. Nevertheless, this does not influence the results, since the lower catenaries will determine the calculations due to their shorter distance from the ground and vegetation. In this sense, a minimum height of the wire above the ground of 10 m was established according to the regulations, as well as a minimum distance to the vegetation of 4.2 m.

As previously mentioned, the entire process was carried out for the 53 km of the power line.

The risk areas obtained in the forest area are shown in Figure 8 and are distributed as follows:

- Three risk areas were obtained based on the height risk (i.e., vegetation under the power line with a distance below 4.2 m). The total area was 256 m^2, and the average area of each zone was 85 m^2. The minimum distance to the vegetation for the three zones was 1.73 m, 2.19 m and 3.54 m.
- Fifteen risk areas were obtained based on the distance risk (i.e., vegetation located on the sides with a distance below 4.2 m). The total area was 647.9 m^2, and the average area of each zone was 43.2 m^2. The minimum distance to the vegetation for these zones varied from 2.37 m to 4.2 m, and the average value was 3.98 m, so they were very close to the limit for not being considered as risk areas.
- Seventy-three risk areas were obtained based on the fall risk (i.e., when the distance of the fallen vegetation is less than 4.2 m [2]). The total area was 1808 m^2, and the average area of each zone was 24.8 m^2, so in this case these risk areas corresponded to small and isolated zones. The minimum distance ranged from 0 m (i.e., case where the vegetation would touch the wire) to 3 m. This case represents a higher risk than the other two, since the number of areas considered and the lower distance values were significant. In any event, this risk will be conditioned on the fall of the vegetation.

3.3. Results for Self-Generated Drone LiDAR Data

The higher point density of the data obtained from the drone flight made it possible to classify the class wires into different wire groups. In this way, the twofold approach for estimating the catenary (real vs. theoretical) was used and compared. First, the real catenary geometry corresponding to the drone flight was estimated from the point cloud, whereas the theoretical catenary based on the maximum sag hypothesis was also applied. In both cases, a minimum distance of 4.2 m was used following the regulations.



Figure 8. Risk areas obtained with public airborne LiDAR data using the approach based on the theoretical catenary using the maximum sag hypothesis.

The risk areas obtained in this case from the theoretical catenary based on the maximum sag hypothesis are shown in Figure 9 and are distributed as follows:

- No risk areas were obtained based on the height risk (i.e., vegetation under the power line with a distance below 4.2 m).
- No risk areas were obtained based on the distance risk (i.e., vegetation on the sides).
- Eighty-nine risk areas were obtained based on the fall risk (i.e., when the distance of the fallen vegetation is less than 4.2 m). The total area was 430 m^2, and the average area of each zone was 7.4 m^2. The minimum distance ranged from 0 m (case where the vegetation would touch the wire) to 2.96 m.



Figure 9. Risk areas obtained with drone LiDAR data using the theoretical catenary based on the maximum sag hypothesis.

For the calculation of the real catenary geometry from the wire groups using the point cloud, the risk areas shown in Figure 10 were obtained and distributed as follows:

- No risk areas were obtained based on the height risk (i.e., vegetation under the power line with a distance below 4.2 m).
- No risk areas were obtained based on the distance risk (i.e., vegetation on the sides with a distance below 4.2 m).
- Thirty-four risk areas were obtained based on the fall risk (i.e., when the distance of the fallen vegetation is less than 4.2 m). The total area was 145 m^2, and the average area of each zone was 4.3 m^2. The minimum distance ranged from 0 m (case where the vegetation would touch the wire) to 2.95 m.



Figure 10. Risk areas obtained with drone LiDAR data from the estimation of wire groups using the point cloud.

3.4. Discussion

To analyse the differences between the two methods and to verify the validity of the calculations made with the public airborne LiDAR data, a summary and comparison of the results is shown in Table 3.

Table 3. Risk analysis and comparison corresponding to each type of data and the three different geometric risks. * Surface units in m^2. MSH refers to theoretical catenary estimated based on the maximum sag hypothesis. rCatenary refers to the real catenary computed from the geometry extracted from the point clouds using drone LiDAR data.

Risk Type / Data Type	Height		Distance		Fall	
	Number of Areas	Total Surface *	Number of Areas	Total Surface *	Number of Areas	Total Surface *
Airborne LiDAR—MSH	3	256	15	647.9	73	1808
Drone LiDAR—MSH	0	0	0	0	89	430
Drone LiDAR—rCatenary	0	0	0	0	34	145

On the one hand, when comparing the case of maximum sag hypothesis for public airborne LiDAR data and self-generated drone LiDAR data, a greater number and more unfavourable risk areas were obtained in the first case. This can be explained from the point of view that it is assumed that the minimum wire height above ground is 10 m (value obtained from the design standards for the analysed power line characteristics).

On the contrary, when the drone flight was processed, the real height of the wire for the maximum sag hypothesis was higher, changing in each section but close to 1 m. In particular, for the height and distance risks, some areas appeared for the analysis with public airborne LiDAR data, while no results were found when processing using drone LiDAR data. Nevertheless, the processing of public airborne LiDAR data achieved its purpose of being a good preventive measure. Although both the number of areas and the total surface of these areas were smaller, risk areas were found based on the fall risk in both datasets (airborne and drone LiDAR).

On the other hand, when comparing the results of risk areas using drone LiDAR data and the two ways of computing the catenary (i.e., theoretical vs. real), it can be said that the results were as expected. A larger number of areas and larger surface were obtained in the case of the theoretical catenary based on the maximum sag hypothesis. In this case, the results were more unfavourable because the theoretical catenary was also more unfavourable.

Note that the risk areas obtained under the maximum sag hypothesis were the final results that should lead to an analysis using the Geographical Information System (GIS) to plan preventive measures, since this analysis guaranteed the most unfavourable scenario.

A more detailed analysis was carried out for the most conflictive section between pylons with the highest number of risk areas. Figure 11 shows the visual comparison for the three processing types: (a) public airborne LiDAR data and theoretical catenary; (b) self-generated drone LiDAR data and theoretical catenary; (c) self-generated drone LiDAR data and real catenary. The largest risk area was selected in order to compare the surface areas for each case, and statistical values such as the range of distances or the average were computed. The surface area corresponding to this largest risk area shown in Figure 11 was 63.99 m^2 in the case of public airborne LiDAR data, 11.50 m^2 in the case of drone LiDAR data using the theoretical catenary based on the maximum sag hypothesis, and 0.50 m^2 for the same data using the real catenary at the time of drone flight.

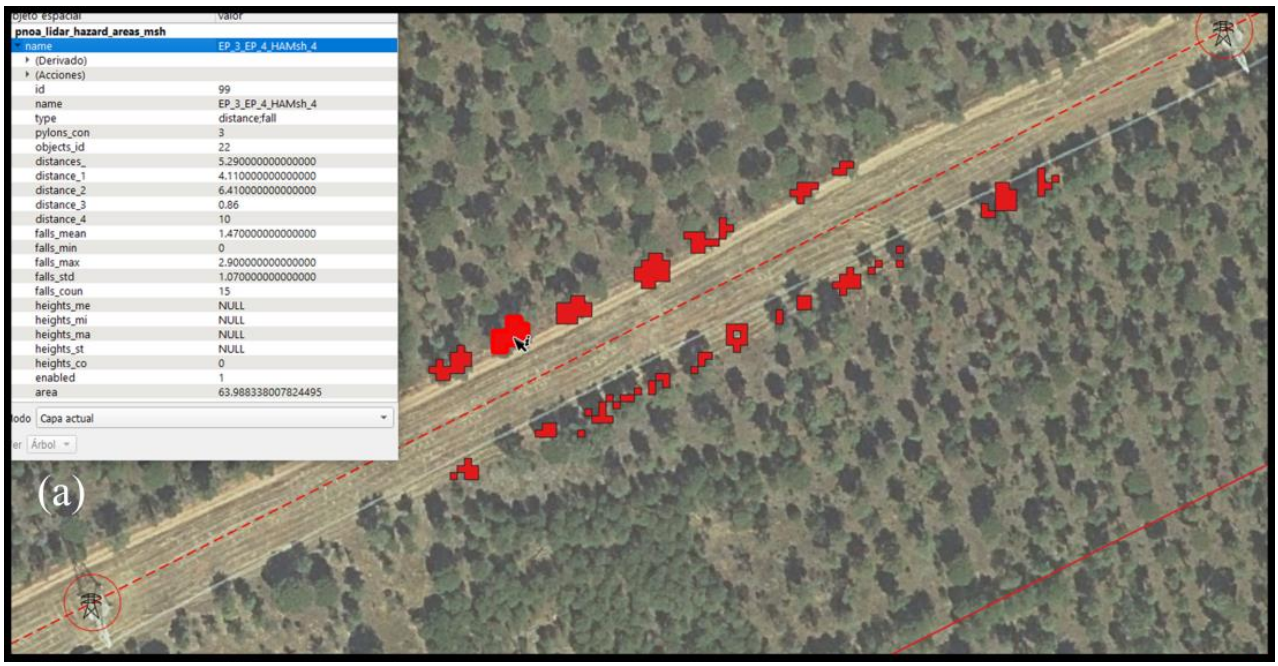


Figure 11. *Cont.*

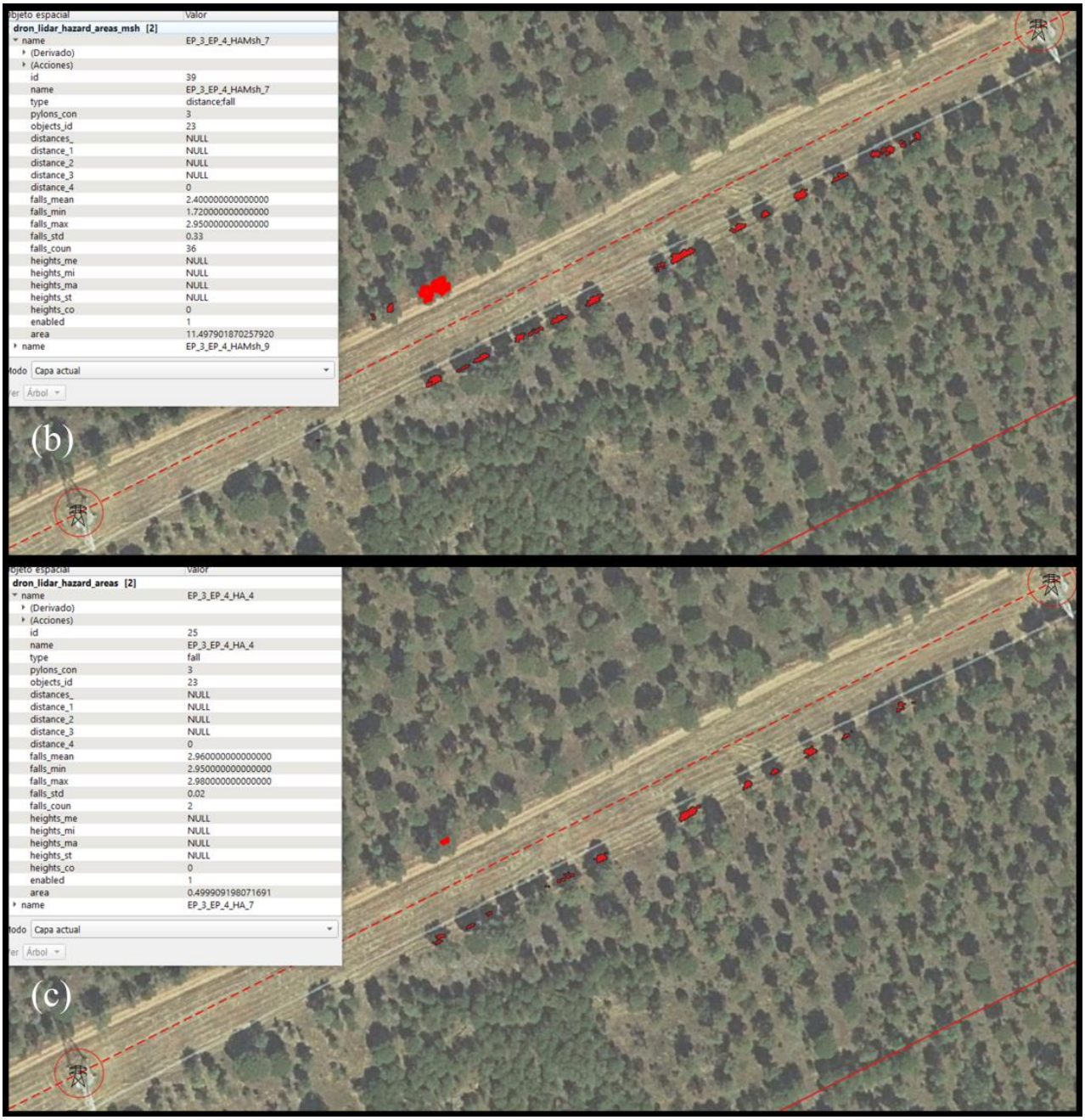


Figure 11. Comparison of risk areas obtained for the three processing types: (**a**) Public airborne LiDAR data with theoretical catenary; (**b**) drone LiDAR data with theoretical catenary; and (**c**) drone LiDAR data with real catenary.

4. Conclusions

This work aimed to automate the calculation of forest fire risk areas along high-voltage power lines. To this end, a methodology focused on geometric analysis was developed using public and self-generated LiDAR data.

First, an analysis of a 53 km section of a high-voltage power line was carried out in order to detect the risk areas using a conservative approach that considered the worst scenario. In this analysis, the theoretical catenary was estimated using the maximum sag hypothesis. The results showed the presence of risk areas along a 2200 m section that crossed a forest area. Although the risk areas were being overestimated, this initial approximation made it possible to delimit the study area for a drone flight in order to carry out a coarse-to-fine analysis. This significantly reduced costs due to the higher cost of drone

flights and the free availability of public airborne LiDAR data. In addition, it was possible to automate the processing for a preliminary analysis of very large territories, which could be reanalysed for new editions of public airborne LiDAR flights.

The analysis of the section with risk areas using drone LiDAR data was carried out using a twofold approach for the calculation of the catenary. On the one hand, its real geometry was estimated using the point cloud, obtaining a smaller number of risk areas due to the fact that the conditions of the wires at the time of the flight were not the most unfavourable. On the other hand, the estimation of the theoretical catenary based on the maximum sag hypothesis was also used, and the results in this case showed better agreement with the analysis of public airborne LiDAR data. Nevertheless, the number of risk areas and their combined surface were smaller, as the wire geometry was adapted to the pylons, showing more favourable conditions than the minimum restrictions of the design regulations.

This analysis demonstrated the importance of drone LiDAR data to provide insight into the areas detected in the preliminary analysis, as well as the importance of using the theoretical catenary based on the maximum sag hypothesis, since the power line conditions may vary, and thus, the data will be available in the most unfavourable situation. In addition, these results can be integrated within a GIS including any other type of information such as the location and age of the power line infrastructure, so these values can perform as weight factors in the risk analysis (e.g., those power lines closer to urban areas will provide a lower risk factor due to the presence of humans; those power lines that are older will present a higher risk due to the possible worse state of the wires). For this purpose, the integrated vegetation growth model allows establishing prevention measures for these forest areas, especially those that are close to urban areas. In this sense, future work will focus on the validation of other vegetation growth models to improve the predictions, which could help to identify risk areas in wildland–urban interface (WUI) zones. It is also intended to integrate into the methodology the automation of other processes such as the automatic detection of pylons in orthophotos or the calculation of their height from their shadows for greater precision in preliminary studies.

Author Contributions: Conceptualization, D.H.-L., J.L.-R., M.A.M. and D.G.-A.; methodology, D.H.-L., J.L.-R., M.A.M. and D.G.-A.; software, D.H.-L.; validation, D.H.-L., J.L.-R., M.A.M. and D.G.-A.; formal analysis, D.H.-L., J.L.-R., M.A.M. and D.G.-A.; investigation, D.H.-L. and J.L.-R.; resources, D.H.-L., J.L.-R., M.A.M. and D.G.-A.; data curation, D.H.-L., J.L.-R., M.A.M. and D.G.-A.; writing—original draft preparation, J.L.-R.; writing—review and editing, D.H.-L., J.L.-R., M.A.M. and D.G.-A.; visualization, D.H.-L., J.L.-R., M.A.M. and D.G.-A.; supervision, D.H.-L., J.L.-R., M.A.M. and D.G.-A.; project administration, D.H.-L., M.A.M. and D.G.-A.; funding acquisition, D.H.-L., M.A.M. and D.G.-A. All authors have read and agreed to the published version of the manuscript.

Funding: This work is financially supported by the European Project H2020 TREEADS: A Holistic Fire Management Ecosystem for Prevention, Detection and Restoration of Environmental Disasters. REF: 101036926.

Data Availability Statement: Not applicable.

Conflicts of Interest: The authors declare no conflict of interest.

References

1. Red Eléctrica: Gestor de la Red y Transportista. Available online: https://www.ree.es/es/actividades/gestor-de-la-red-y-transportista (accessed on 20 February 2023).
2. Real Decreto 223/2008, de 15 de febrero, por el que se aprueban el Reglamento sobre condiciones técnicas y garantías de seguridad en líneas eléctricas de alta tensión y sus instrucciones técnicas complementarias ITC-LAT 01 a 09. 2008. Available online: https://www.boe.es/eli/es/rd/2008/02/15/223 (accessed on 22 March 2023).
3. Chen, Y.; Lin, J.; Liao, X. Early detection of tree encroachment in high voltage powerline corridor using growth model and UAV-borne LiDAR. *Int. J. Appl. Earth Obs. Geoinf.* **2022**, *108*, 102740. [CrossRef]
4. Rodríguez, A.P.; Gil, D.C. Impactos de tendidos eléctricos de alta tensión: Análisis, evaluación y restauración. *Rev. Digit. Cedex* **2016**, *182*, 79.

5. Miller, C.; Plucinski, M.; Sullivan, A.; Stephenson, A.; Huston, C.; Charman, K.; Prakash, M.; Dunstall, S. Electrically caused wildfires in Victoria, Australia are over-represented when fire danger is elevated. *Landsc. Urban Plan.* **2017**, *167*, 267–274. [CrossRef]
6. Mitchell, J.W. Power line failures and catastrophic wildfires under extreme weather conditions. *Eng. Fail. Anal.* **2013**, *35*, 726–735. [CrossRef]
7. Cubo, J.E.; Enríquez; Gallar, J.J.; Jemes, V.; López, M.; Mateo, M.L.; Muñoz, A.; Parra, P.J. *Los incendios Forestales en España. Decenio 2001–2010*; Ministerio de Agricultura, Alimentación y Medio Ambiente: Madrid, Spain, 2012; Volume 38.
8. Tsurutani, B.T.; Gonzalez, W.D.; Lakhina, G.S.; Alex, S. The extreme magnetic storm of 1–2 September 1859. *J. Geophys. Res. Space Phys.* **2003**, *108*. [CrossRef]
9. Phillips, T. The Great Geomagnetic Storm of May 1921. 2020. Available online: https://spaceweatherarchive.com/2020/05/12/the-great-geomagnetic-storm-of-may-1921/ (accessed on 22 March 2023).
10. Wallace, D. *Massive Geomagnetic Storm: Coronal Mass Ejection From the Sun Could Knock Out the Power Grid and Internet*; Mississippi State University: Starkville, MS, USA, 2022.
11. Odenwald, S. The Day the Sun Brought Darkness. 2017. Available online: https://www.nasa.gov/topics/earth/features/sun_darkness.html (accessed on 22 March 2023).
12. Vyklyuk, Y.; Radovanović, M.M.; Stanojević, G.; Petrović, M.D.; Ćurčić, N.B.; Milenković, M.; Malinović Milićević, S.; Milovanović, B.; Yamashkin, A.A.; Milanović Pešić, A. Connection of Solar Activities and Forest Fires in 2018: Events in the USA (California), Portugal and Greece. *Sustainability* **2020**, *12*, 10261. [CrossRef]
13. Ministerio de Industria, T.y.C. Instrucción Técnica Complementaria ITC-LAT 07: Líneas aéreas con conductores desnudos. 2019. Available online: https://www.boe.es/buscar/act.php?id=BOE-A-2008-5269#itclat07 (accessed on 22 March 2023).
14. Ahmad, J.; Malik, A.S.; Xia, L.; Ashikin, N. Vegetation encroachment monitoring for transmission lines right-of-ways: A survey. *Electr. Power Syst. Res.* **2013**, *95*, 339–352. [CrossRef]
15. Qayyum, A.; Malik, A.S.; Saad, M.N.M.; Iqbal, M.; Abdullah, M.F.; Abdullah, T.A.R.B.T.; Ramli, A.Q. Power LinesVegetation enchroachment monitoring based on Satellite Stereo images using stereo matching. In Proceedings of the 2014 IEEE International Conference on Smart Instrumentation, Measurement and Applications (ICSIMA), Kuala Lumpur, Malaysia, 25 November 2014; pp. 1–5.
16. Oliveira, E.R.; Disperati, L.; Alves, F.L. A new method (MINDED-BA) for automatic detection of burned areas using remote sensing. *Remote Sens.* **2021**, *13*, 5164. [CrossRef]
17. Azevedo, F.; Dias, A.; Almeida, J.; Oliveira, A.; Ferreira, A.; Santos, T.; Martins, A.; Silva, E. Lidar-based real-time detection and modeling of power lines for unmanned aerial vehicles. *Sensors* **2019**, *19*, 1812. [CrossRef]
18. Takhirov, S.M.; Israilov, M.S. Reduction of wildfire hazard by automated monitoring of vegetation interference with power lines: Point cloud analysis combined with cable mechanics. *J. Civ. Struct. Health Monit.* **2020**, *10*, 947–956. [CrossRef]
19. PNOA-LiDAR. Available online: https://pnoa.ign.es/el-proyecto-pnoa-lidar (accessed on 20 February 2023).
20. Cabo, C.; Del Pozo, S.; Rodríguez-González, P.; Ordóñez, C.; González-Aguilera, D. Comparing terrestrial laser scanning (TLS) and wearable laser scanning (WLS) for individual tree modeling at plot level. *Remote Sens.* **2018**, *10*, 540. [CrossRef]
21. Gonzalez-Aguilera, D.; Rodriguez-Gonzalvez, P. Drones—An Open Access Journal. *Drones* **2017**, *1*, 1. [CrossRef]
22. Kramer, H.A.; Collins, B.M.; Lake, F.K.; Jakubowski, M.K.; Stephens, S.L.; Kelly, M. Estimating ladder fuels: A new approach combining field photography with LiDAR. *Remote Sens.* **2016**, *8*, 766. [CrossRef]
23. Lyalin, K.S.; Biryuk, A.A.; Sheremet, A.Y.; Tsvetkov, V.K.; Prikhodko, D.V. UAV synthetic aperture radar system for control of vegetation and soil moisture. In Proceedings of the 2018 IEEE Conference of Russian Young Researchers in Electrical and Electronic Engineering (EIConRus), Moscow and St. Petersburg, Russia, 29 January–1 February 2018; pp. 1673–1675.
24. Finn, M.P.; Lewis, M.; Bosch, D.D.; Giraldo, M.; Yamamoto, K.; Sullivan, D.G.; Kincaid, R.; Luna, R.; Allam, G.K.; Kvien, C. Remote sensing of soil moisture using airborne hyperspectral data. *GIScience Remote Sens.* **2011**, *48*, 522–540. [CrossRef]
25. Kandanaarachchi, S.; Anantharama, N.; Munoz, M.A. Early detection of vegetation ignition due to powerline faults. *IEEE Trans. Power Deliv.* **2020**, *36*, 1324–1334. [CrossRef]
26. Vadrevu, K.P. Fire danger indices and methods: An appraisal. In *Biomass Burning in South and Southeast Asia*; CRC Press: Boca Raton, FL, USA, 2021; pp. 201–232.
27. Xu, K.; Zhang, X.; Chen, Z.; Wu, W.; Li, T. Risk assessment for wildfire occurrence in high-voltage power line corridors by using remote-sensing techniques: A case study in Hubei Province, China. *Int. J. Remote Sens.* **2016**, *37*, 4818–4837. [CrossRef]
28. Chuvieco, E.; Aguado, I.; Jurdao, S.; Pettinari, M.L.; Yebra, M.; Salas, J.; Hantson, S.; de la Riva, J.; Ibarra, P.; Rodrigues, M. Integrating geospatial information into fire risk assessment. *Int. J. Wildland Fire* **2012**, *23*, 606–619. [CrossRef]
29. Liang, Y.; Zhou, L.; Chen, J.; Huang, Y.; Wei, R.; Zhou, E. Monitoring and risk assessment of wildfires in the corridors of high-voltage transmission lines. *IEEE Access* **2020**, *8*, 170057–170069. [CrossRef]
30. Germano, F.; Duarte, L.; Teodoro, A.C. Integration of geospatial information in a GIS software to estimate the forest fire risk. In Proceedings of the Earth Resources and Environmental Remote Sensing/GIS Applications XII, 12 September 2021; Volume 11863, pp. 53–67.
31. Golinelli, E.; Perini, U.; Barberis, F.; Musazzi, S. A Laser Scanning System for Sag Detection on the Overhead Power Lines: In Field Measurements. In *Sensors*; Springer: Berlin/Heidelberg, Germany, 2014; pp. 311–314.

32. Tan, J.; Zhao, H.; Yang, R.; Liu, H.; Li, S.; Liu, J. An Entropy-Weighting Method for Efficient Power-Line Feature Evaluation and Extraction from LiDAR Point Clouds. *Remote Sens.* **2021**, *13*, 3446. [CrossRef]
33. Isenburg, M. LAStools-Efficient Tools for LiDAR Processing. 2020. Available online: http://www.cs.unc.edu/~isenburg/lastools/ (accessed on 20 February 2023).
34. PNOA-LiDAR Specifications. Available online: https://pnoa.ign.es/web/portal/pnoa-lidar/especificaciones-tecnicas (accessed on 20 February 2023).
35. Centro Nacional de Información Geográfica (CNIG). Available online: https://centrodedescargas.cnig.es (accessed on 20 February 2023).
36. American Society for Photogrammetry and Remote Sensing. *LAS Specification 1.4-R15*; ASPRS The Imaging & Geospatial Information Society: Bethesda, MD, USA, 2019.
37. SIOSE Alta Resolución. Available online: https://www.siose.es/siose-alta-resolucion (accessed on 20 February 2023).
38. Han, X.-F.; Jin, J.S.; Wang, M.-J.; Jiang, W.; Gao, L.; Xiao, L. A review of algorithms for filtering the 3D point cloud. *Signal Process. Image Commun.* **2017**, *57*, 103–112. [CrossRef]
39. Breiman, L. Random forests. *Mach. Learn.* **2001**, *45*, 5–32. [CrossRef]
40. CGAL 5.5.2—Classification. User Manual. Available online: https://doc.cgal.org/latest/Classification/index.html (accessed on 15 March 2023).
41. Walk, S. *ETH Zurich Random Forest Template Library*; ETH Zurich, Department of Civil, Environmental and Geomatic Engineering, Institute of Geodesy and Photogrammetry: Zurich, Switzerland, 2014.
42. PointCloudLibrary. Euclidean Cluster Extraction. Available online: https://pcl.readthedocs.io/en/latest/cluster_extraction.html (accessed on 20 February 2023).
43. Hatibovic, A. Integral calculus usage for conductor length determination on the basis of known maximal sag of a parabola. *Period. Polytech. Electr. Eng. Comput. Sci.* **2012**, *56*, 35–41. [CrossRef]
44. Hatibovic, A. Derivation of equations for conductor and sag curves of an overhead line based on a given catenary constant. *Period. Polytech. Electr. Eng. Comput. Sci.* **2014**, *58*, 23. [CrossRef]
45. *Calculation of Sag-tension for Overhead Power Lines*; CIGRE WG B2-12: Klingenberg, Germany, 2016.
46. Forestry Map of Spain. Available online: https://www.miteco.gob.es/es/biodiversidad/temas/inventarios-nacionales/mapa-forestal-espana/mfe_50.aspx (accessed on 20 February 2023).

Disclaimer/Publisher's Note: The statements, opinions and data contained in all publications are solely those of the individual author(s) and contributor(s) and not of MDPI and/or the editor(s). MDPI and/or the editor(s) disclaim responsibility for any injury to people or property resulting from any ideas, methods, instructions or products referred to in the content.